Stable anode interphase enabled use of protic electrolytes in sodium metal batteries

Downloaded from: https://research.chalmers.se, 2025-09-25 05:43 UTC

Citation for the original published paper (version of record):
Li, Y., Hosaka, T., Maibach, J. et al (2025). Stable anode interphase enabled use of protic electrolytes in sodium metal batteries. Energy Storage Materials, 82.
http://dx.doi.org/10.1016/j.ensm.2025.104566

N.B. When citing this work, cite the original published paper.

research.chalmers.se offers the possibility of retrieving research publications produced at Chalmers University of Technology. It covers all kind of research output: articles, dissertations, conference papers, reports etc. since 2004. research.chalmers.se is administrated and maintained by Chalmers Library

(article starts on next page)

Energy Storage Materials 82 (2025) 104566

Contents lists available at ScienceDirect

Energy Storage Materials

journal homepage: www.elsevier.com/locate/ensm

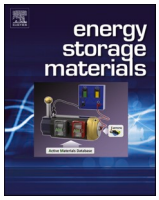

Stable anode interphase enabled use of protic electrolytes in sodium metal batteries

Yihu Li [a], Tomooki Hosaka [a], Julia Maibach [a], Patrik Johansson [a,b,*]

[a] Department of Physics, Chalmers University of Technology, 41296 Göteborg, Sweden
[b] ALISTORE-ERI, CNRS FR 3104, Hub de l'Energie, 80039 Amiens Cedex, France

ARTICLE INFO

Keywords:
Sodium batteries
Electrolyte
Protic solvent
Sodium metal anode
Interphase

ABSTRACT

Sodium metal batteries based on liquid electrolytes are currently limited to using aprotic solvents, such as carbonate esters and ethers. This as protic solvents fundamentally have proton dissociation due to prevalent hydrogen bonding, leading to undesirable reactivity with the sodium metal anode. Our working hypothesis is that this reactivity can be controlled and reduced by replacing/disrupting the hydrogen bonding with other interactions. We present here the viability by using N-methyl-acetamide as an electrolyte solvent for sodium metal batteries, to which both Na^+ cations and $[FSI]^-$ anions, from the NaFSI electrolyte salt used, can interact to modify the N—H bond strength. Combined with the formation of aggregates by careful composition control, the passivation of sodium metal anodes is effectively improved. Furthermore, distinctly different solid electrolyte interphases are formed, as compared to when using a conventional organic electrolyte, and excellent cycling stability of a full cell using $Na_3V_2(PO_4)_3$ as cathode is demonstrated, reaching an average Coulombic efficiency of 99.9 %. Overall, we show that protic solvents, given controlled proton activity, offer another route to possibly achieve practical sodium metal batteries.

1. Introduction

Lithium-ion batteries (LIBs) are the leading choice for applications like electric vehicles and grid storage, but alternative battery technologies are gaining momentum. Sodium-ion batteries (SIBs) have made significant strides owing to the abundance and availability of sodium, as well as their drop-in compatibility with LIB manufacturing infrastructure [1]. For example, integrating SIBs and LIBs cells, hybrid battery packs have been developed for extended-range hybrid vehicles [2]. Yet, improvements in energy density are needed for SIBs. The mainstream anode active material used, hard carbon, faces challenges from large first-cycle irreversible capacity losses and high production costs [3]. Moving to sodium metal anodes, with a high specific capacity of 1166 mAh/g, is a promising alternative [4], but so far its intrinsically high chemical and electrochemical reactivity poses challenges, especially as to finding stable electrolytes.

Electrolytes for sodium metal batteries (SMBs) can be based on organic solvents [5], polymers [6], ionic liquids [7], or inorganic compounds [8]. Traditionally, (aprotic) organic liquid electrolytes have been favored because of their cost effectiveness and ease of production. Protic organic solvent-based electrolytes have been far less in focus, even though they can form deep eutectic solvents (DESs) that exhibit low vapor pressure, wide liquid range, and non-flammability. But the protons of their O—H/N—H groups can dissociate and react with sodium metal [4,9] Brandt et al., however, demonstrated that the labile proton of the cation in dry protic ionic liquids is not "free" and that this cation is not subject to reversible protonation–deprotonation [10]. Hence, controlling proton activity could make protic electrolytes feasible for SMBs. Considering that protic solvents are enriched with hydrogen bonds (HBs), this can be harnessed to enhance interactions to stabilize the electrolyte. In this context anions from sodium salts can act as HB acceptors, while the protic solvents themselves can serve as HB donors. Moreover, highly concentrated electrolytes (HCEs) can further improve the stability towards sodium metal anodes [11–12]. For example, De Sloovere et al. mixed sodium bis(trifluoromethanesulfone)imide (NaTFSI) and N-methyl-acetamide (NMA) and found a decreased reactivity with sodium metal simply by increasing the electrolyte salt concentration [13]. In a later study from the same group, NaTFSI was replaced with sodium bis(fluorosulfonyl)imide (NaFSI) to further increase the electrolyte salt concentration [14]. Even though their Na//Na symmetric cell showed a prolonged cycle life [14], this alone does not conclusively prove compatibility with a sodium metal anode – as the two

* Corresponding author at: Department of Physics, Chalmers University of Technology, 41296 Göteborg, Sweden.
E-mail address: patrik.johansson@chalmers.se (P. Johansson).

https://doi.org/10.1016/j.ensm.2025.104566
Received 11 June 2025; Received in revised form 18 August 2025; Accepted 27 August 2025
Available online 28 August 2025
2405-8297/© 2025 The Authors. Published by Elsevier B.V. This is an open access article under the CC BY license (http://creativecommons.org/licenses/by/4.0/).

electrodes act as almost inexhaustible reservoirs of Na and side-reactions can thus still be plentiful. The problematic reactivity arises not only from "free" NMA in the bulk of the electrolyte, but also from solvated NMA that becomes "free" after cation de-solvation at the electrolyte-sodium metal interface.

Here, our working hypothesis is that using an HCE, coupled with modulation of the proton activity through reinforcement of the N–H/O—H bond in protic solvents, is key to forming a stable solid electrolyte interphase (SEI) that effectively suppresses the reactivity. We employ electrolytes composed of NaFSI in NMA, leveraging the strong dissociation of the salt to enhance the interactions with NMA, which in turn regulate proton activity [15–17]. We use a range of both experimental and computational methods to probe the local cation coordination, including the propensity of HB, as well as the interfacial stability, and finally the cycling performance of full cells.

2. Results and discussion

We start by formulating HCEs and studying their local coordination and ionic interactions in detail using both Raman and Fourier-transform infrared (FTIR) spectroscopy, and by molecular dynamics (MD) simulations. Subsequently, we assess the impact of the electrolyte composition on the interphase formation and properties through Coulometric titration, to probe the sodium metal passivation, by X-ray photoelectron spectroscopy (XPS), to determine the surface composition and infer differences in SEI thickness, by galvanostatic cycling, to validate the SEI stability in practice. Finally, we evaluate the cycling performance of Na/electrolyte/$Na_3V_2(PO_4)_3$ full cells.

3. Electrolyte local structure: ion pairing, aggregate formation, and N—H bond reinforcement

In HCEs, as well as in electrolytes in general, the displacement of solvent, here NMA, from the Na^+ cation first solvation shell by anions, here $[FSI]^-$, via increasing the salt concentration, here NaFSI, *i.e.* increasing the salt:solvent ratio, here NaFSI:NMA, can excellently be monitored using Raman spectroscopy. We here use the peak corresponding to the S-N-S bending mode of $[FSI]^-$, which progressively moves to higher Raman shifts as ion-pairs and higher aggregates are formed (Fig. 1a) [18–19]. Specifically, "free" $[FSI]^-$ is found at *ca.* 726 cm^{-1}, as observed for the NaFSI:NMA=1.0:30.0 electrolyte, but for higher NaFSI concentrations (ratios 1.0:1.5, 1.0:1.2 and 1.0:1.0), contact ion-pairs (CIPs), at *ca.* 736–737 cm^{-1}, and higher aggregates (AGG-I and AGG-II), at *ca.* 746–755 cm^{-1}, are the main features (Fig. 1b and S1). The CIPs decline from *ca.* 30 % to *ca.* 19 %, whereas both AGG-I and AGG-II grow by *ca.* 5–10 % each (Fig. 1b), which arguably may induce an anion-derived SEI, with improved stability [11].

Moving to the MD simulations these corroborate the formation of aggregates as function of salt concentration, as shown by increased partial coordination numbers (pCNs) of Na-O_{FSI} (Fig. 1c). In addition, the conjugation in NMA enables Na-O_{NMA} contributions, but as a function of salt concentration, NMA tends to be less present in the cation first solvation shell, as indicated by decreasing Na-O_{NMA} pCNs as we move from NaFSI:NMA=1.0:1.5 to 1.0:1.0 (Fig. 1d). Within that shell, O_{NMA} still approaches Na^+ more closely than O_{FSI} does (Figure S2), indicating the strong Na-NMA affinity even though fewer NMA molecules are present overall.

In addition to the less pronounced NMA coordination, the FTIR

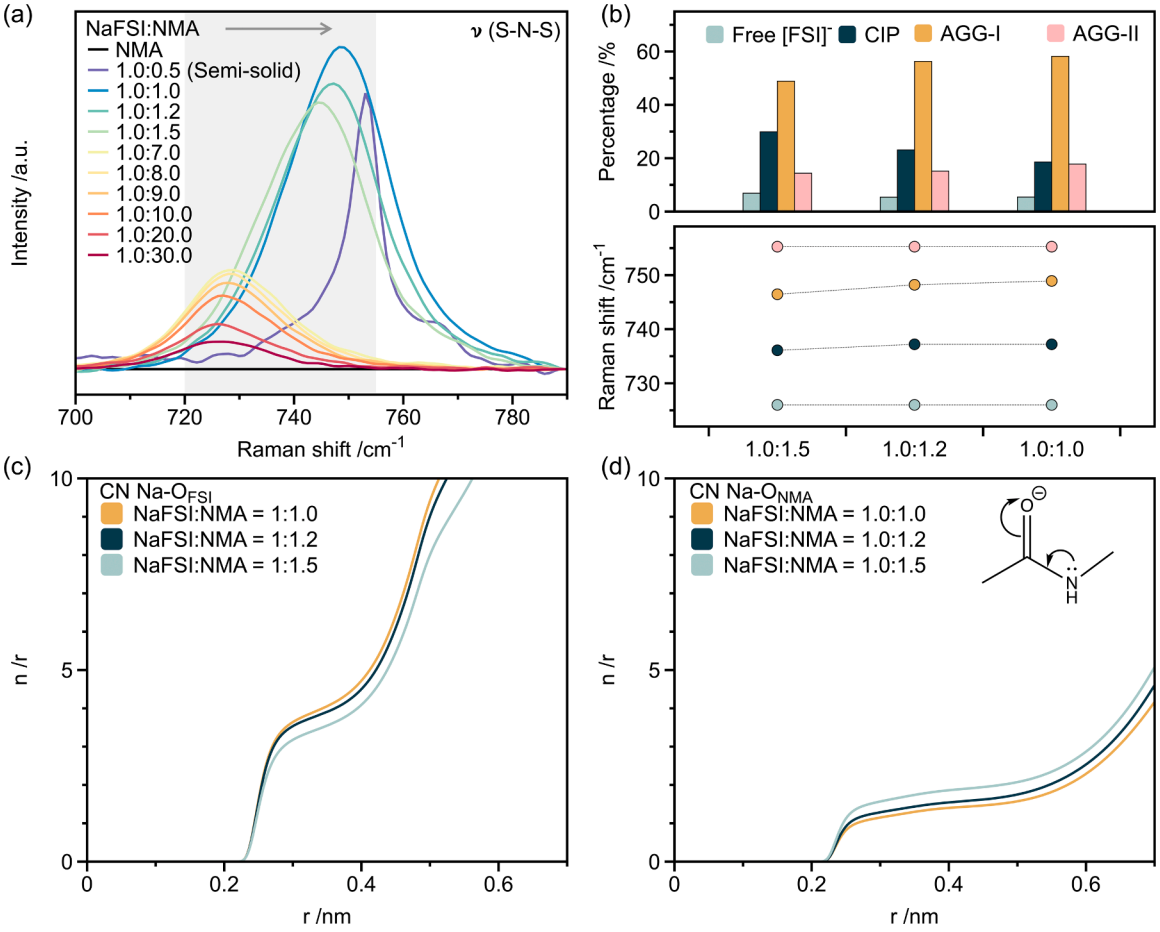

Fig. 1. (a) Raman spectra in the region of the peak of the S-N-S bending mode of $[FSI]^-$, (b) speciation and Raman shifts of "free" $[FSI]^-$, CIPs, AGG-I and AGG-II, and pCNs from MD simulation: (c) Na-O_{FSI} and (d) Na-O_{NMA} *vs.* distance (r). All as function of salt concentration.

spectra (Fig. 2) show the H-bonded N—H stretching mode peak at *ca.* 3290 cm^{-1} in pure NMA [20] and a new non-H-bonded N—H peak at *ca.* 3425 cm^{-1} in the electrolytes. Both display blue shifts with increasing salt concentration, suggesting a shortening or strengthening of the N—H bond, [21–22] probably originating in that Na^+ interacts with O_{NMA}, competing with the N—H_{NMA} interaction. This competition thus disrupts the intra- and intermolecular HB network, as further confirmed by the decreasing number of HBs per H_{NMA} (Figure S3a), and thereby ultimately reducing the probability of proton dissociation. Although also O_{FSI} can interact with N—H_{NMA}, [23] potentially weakening the bond, the electronegativity of O_{FSI} is largely neutralized by Na^+ in HCEs. Combined with steric hindrances, this collectively results in weaker and fewer interactions between N—H_{NMA} and O_{FSI}; with H_{NMA}-O_{FSI} distance longer than H_{NMA}-O_{NMA} (Figure S3b), on average only *ca.* 0.5 O_{FSI} and almost no F_{FSI} drag H from N—H_{NMA} (Figure S4). Therefore, the overall effect is a strengthening of the N—H bond as a function of salt concentration.

4. Passivation of sodium metal

We evaluate the passivation of the sodium metal anode by Coulometric titration, to characterize the extent of side-reactions between Na and the electrolytes [24]. The initial cycle (Fig. 3a) shows that all electrolytes quickly consume *ca.* 10 μAh of titrant, due to vigorous side-reactions. In the following cycles, longer times were required, indicating passivation slowing down side-reactions. The growth rate of the open circuit potential (OCP), however, differs by the electrolytes employed, which demonstrates their different passivating ability. As the electrolyte salt concentration increases from NaFSI:NMA=1.0:1.5 to 1.0:1.0, the passivation improves, as shown by the longer OCP time needed to deplete the sodium titrant. This correlates with the Raman and FTIR spectroscopy data as well as the MD simulation based observations, where increased salt concentration promotes aggregate formation and stronger N—H bonds in NMA, arguably enhancing SEI formation and stability [13]. Benchmarking using a commercial aprotic organic liquid electrolyte, 1.0 M $NaPF_6$ in EC:PC (50:50 w/w), shows that only the NaFSI:NMA=1.0:1.0 electrolyte has a superior passivation across all titration cycles. After the sixth titration, the OCP time of the benchmark electrolyte levels off, which is attributed to the most stable and complete interphase that can be achieved using this electrolyte. By using linear sweep voltammetry (LSV) we confirm that the NaFSI:NMA=1.0:1.0 electrolyte has the best reductive stability (Fig. 3b) and moreover, it also shows the best oxidative stability to *ca.* 4.3 V

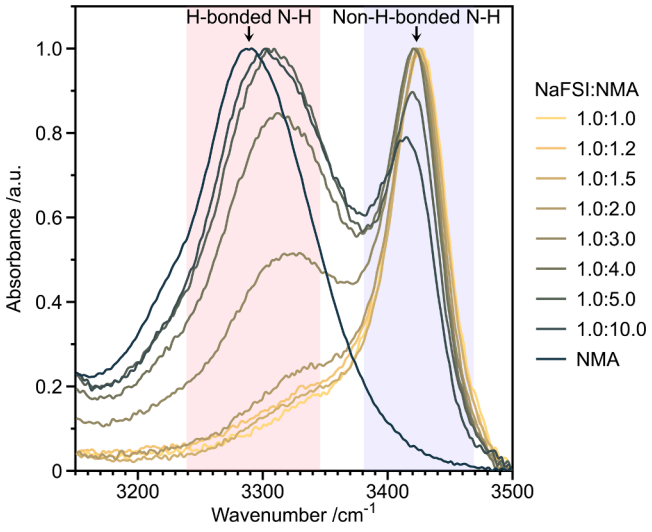

Fig. 2. FTIR spectra of the N—H stretching mode peak of NMA as function of salt concentration and for pure NMA.

(Figure S5). This ratio also exhibits the broadest thermally stable window from -26 °C to 132 °C (Figure S6, Table S1).

5. Interphase on Na

Using XPS we find little elemental surface composition variation as function of electrolyte salt concentration (Fig. 4a and S7). Despite the literature expectations of a salt-derived inorganic SEI with salt concentration increasing [11–12,25], we observe larger C contributions and smaller Na, F, S, and N contributions (Table 1).

Yet, the largest C contribution to the C1s spectra we attribute to a mixture of Na_2CO_3/RCO_2Na/NaOR (Fig. 4b,c and S8), and this increases as salt concentration increases (Fig. 4c and Table 1). Of these species, Na_2CO_3 forms during cycling from RCO_2Na/NaOR (Fig. 4b and S8), whereas RCO_2Na/NaOR are native to the pristine sodium metal surface (Figure S8). This C contribution is thus not an organic one, but an inorganic - as we initially expected. In addition, the NS=O contributions to the N1s spectra originating from $[FSI]^-$ suggest a more inorganic-rich SEI. Notably, the relative intensities of C—N species in the N1s spectra from NMA decrease (Fig. 4d and Table 1), indicating less NMA decomposition. As NMA is the sole source of C, the increased C contribution must come from the native carbonate layer on pristine Na, detectable if the SEI is thin enough. Hence, the larger C contributions do neither indicate NMA degradation nor a more organic SEI.

To determine whether the different SEIs are more organic or inorganic, the stability *vs.* dissolution was evaluated; organic SEIs are more soluble, likely due to their polarity, and inorganic SEIs more stable/insoluble [33–35]. Using Na//Cu cell data and the reduction capacity before and after the pause, the less concentrated electrolyte displays a significant SEI dissolution, but the two more concentrated do not (Figure S10). Thus, the electrochemical data aligns excellently with the XPS results.

Additionally, cyclic voltammetry (CV) reveals that, unlike the NaFSI:NMA=1.0:1.0 electrolyte, the current density in the NaFSI:NMA=1.0:1.5 electrolyte progressively decreases over the first ten cycles (Figure S11). This is likely due to its poorer passivating ability, allowing it to continuously react with Na to form an ever-thickening interphase. The distribution of relaxation times (DRT) analysis of the EIS data support this by an increased time constant for Na^+ passage through the SEI with respect to the 1.0:1.0 electrolyte (Figure S12) [36, 37].

6. Electrochemical assessments

Starting with testing the NaFSI:NMA=1.0:1.0 electrolyte *vs.* $Na_3V_2(PO_4)_2F_3$, Coulombic efficiency was low because electrolyte decomposition contributed to charge capacity above *ca.* 4.3 V (Figure S13), in line with LSV results (Figure S5). To focus on anode interphase, we next assessed NaFSI:NMA electrolytes with $Na_3V_2(PO_4)_3$. The electrolytes with the higher NaFSI concentrations (higher viscosities) showed stepping-up specific capacity during the initial cycles and prolonged stabilization due to slower wetting of the electrodes (Table 2 and Fig. 5a-d) [38]. The cells with the NaFSI:NMA=1.0:1.0 electrolyte stabilized after *ca.* 33 cycles, while those with the NaFSI:NMA=1.0:1.2 electrolyte stabilized faster, after *ca.* 10 cycles, with intermediate stability. The less stable NaFSI:NMA=1.0:1.5 electrolyte degraded from the very first cycle, with significant cell capacity loss by cycle 160 (Table 2 and Fig. 5a, b). Regarding reversibility, the Coulombic efficiency (CE) improved with electrolyte salt concentration, likely due to enhanced stability. As for the lower initial Coulombic efficiency at high salt, this could arise from viscosity-limited wetting and Na^+ transport, which induce polarization and force an early cut-off before full active-material utilization (Figure S14). As wetting improves, early cycles can show CE >100 % (discharge exceeding the prior charge). Indeed, cells with the NaFSI:NMA=1.0:1.0 electrolyte partially rested at 50 °C, enhancing pore infiltration/wetting, achieved faster stabilization as compared to

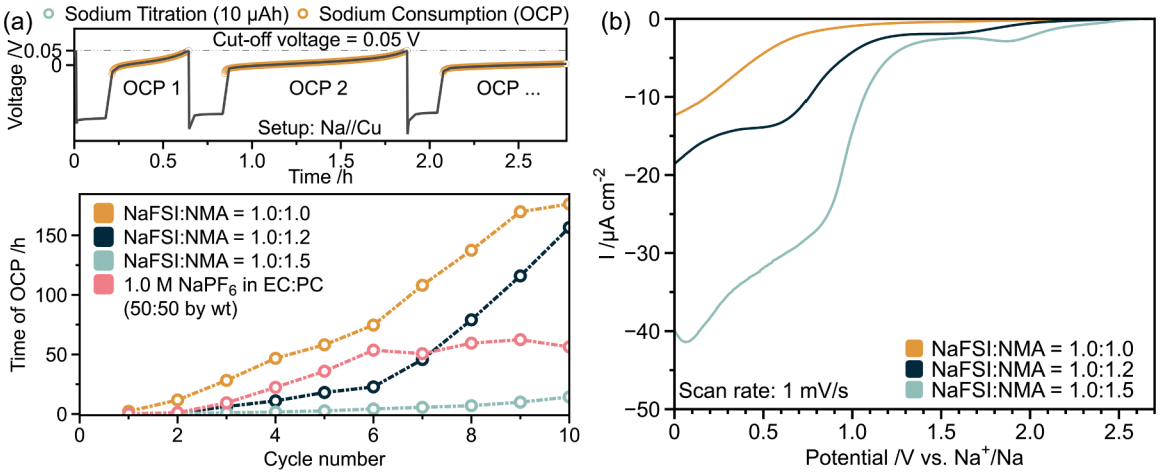

Fig. 3. (a) Coulometric titration time required to exhaust a Na titrant of 10 μAh, and (b) reductive stability of the electrolytes.

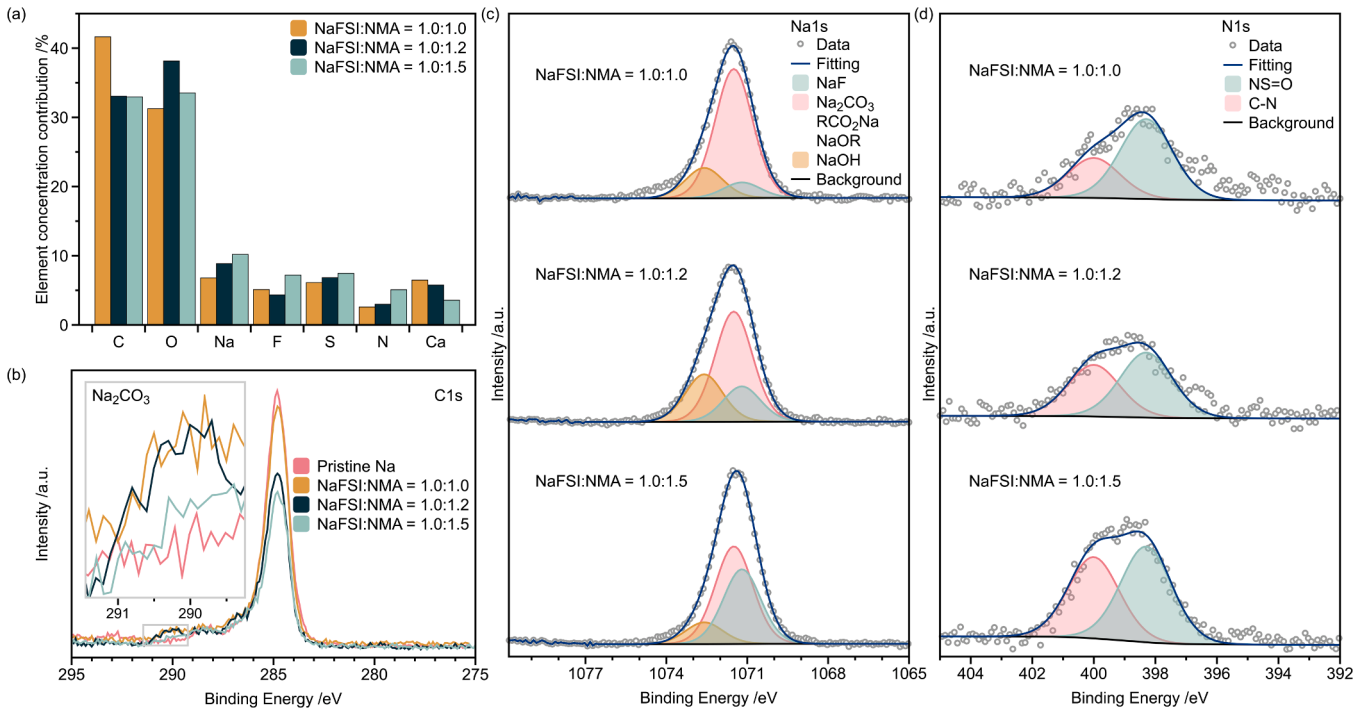

Fig. 4. (a) Relative element concentration contributions to the XPS spectra from Na electrode surfaces after two full cycles in Na//$Na_3V_2(PO_4)_3$ cells at 0.1 C rate, (b) C1s spectra before and after two cycles, and (c) Na1s and (d) N1s spectra (after two cycles), respectively, using the different electrolytes. Although Na_2CO_3 and NaF have similar binding energies in Na1s spectra, we fitted them as separate components because Na_2CO_3 is detected in the C1s region, and NaF appears in the F1s region (Figure S9). In addition, the low N1s signal intensity and high noise increase the fit uncertainty and there is a possible third component at low binding energy.

Table 1
Relative contributions of species to the Na1s and N1s spectra.

	Na1s spectra assignments and relative contributions			N1s spectra assignments and relative contributions	
NaFSI: NMA ratio	Na_2CO_3/ RCO_2Na/NaOR [26–27]	NaF [28]	NaOH [29]	C-N [30–31]	NS=O [32]
	1071.5 eV	1071.2 eV	1072.6 eV	400.0 eV	398.3 eV
1.0:1.5	50 %	39 %	11 %	46 %	54 %
1.0:1.2	57 %	18 %	25 %	44 %	56 %
1.0:1.0	74 %	17 %	9 %	33 %	67 %

Table 2
Galvanostatic cycling performance of Na/NaFSI:NMA/$Na_3V_2(PO_4)_3$ cells.

NaFSI:NMA ratio	Average CE	Stabilized capacity	Capacity at cycle 160	Capacity retention
1.0:1.5	67.8 %	92.7 mAh/g (cycle 1)	73.6 mAh/g	79.4 %
1.0:1.2	96.4 %	89.4 mAh/g (cycle 10)	83.6 mAh/g	93.5 %
1.0:1.0	100.2 %	90.5 mAh/g (cycle 33)	88.4 mAh/g	97.7 %
1.0:1.0*	99.9 %	91.2 mAh/g (cycle 13)	88.7 mAh/g	97.3 %

* Cell rested at 50 °C for 5 h and subsequently 4 h at room temperature. Design principle: use a temperature that speeds wetting without overactivating NMA toward parasitic reactions with sodium.

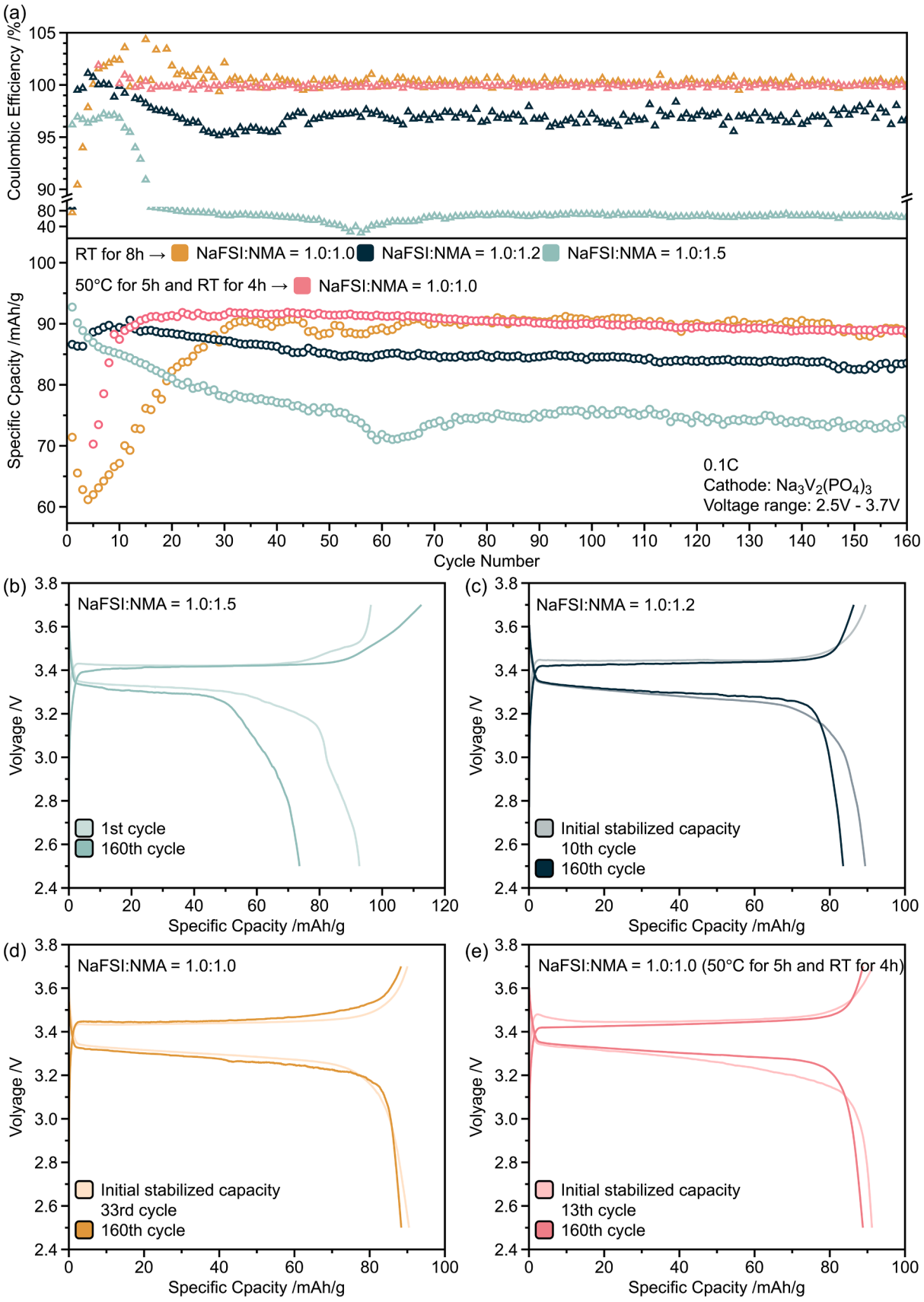

Fig. 5. (a) Cycling performance of Na/NaFSI:NMA/$Na_3V_2(PO_4)_3$ cells at 0.1C, and (b-e) galvanostatic charging and discharging curves for cells at the cycle of their initial stabilized capacity and the 160th cycle with different electrolytes.

those only rested at room temperature (Table 2 and Fig. 5a, e). However, the high viscosity of the electrolytes is still a liability at higher current densities; when the cell is charged at 0.5C, the internal resistance makes it more or less immediately reach the upper cut-off voltage (Figure S15).

7. Conclusions

Our findings demonstrate that NMA indeed is a viable protic solvent for SMBs. The key is to minimize the concentration of "free" solvent at the Na interface and manage the proton dissociation, which collectively dictates the interfacial properties, *e.g.,* by forming a more resistive/passivating SEI. As a result, our full cells with optimized electrolyte salt concentration deliver robust long-term cycling with minimal capacity fade. Combined this opens new avenues for further advancing SMBs and future work should, at least partly, focus on exploring other protic solvents to expand the electrolyte solvent options as well as reducing the viscosity.

CRediT authorship contribution statement

Yihu Li: Writing – original draft, Methodology, Investigation, Formal analysis, Conceptualization. **Tomooki Hosaka:** Writing – review & editing, Supervision. **Julia Maibach:** Writing – review & editing, Supervision. **Patrik Johansson:** Writing – review & editing, Supervision, Resources, Project administration, Funding acquisition, Conceptualization.

Declaration of competing interest

The authors declare that they have no known competing financial interests or personal relationships that could have appeared to influence the work reported in this paper.

Acknowledgements

The authors gratefully acknowledge Dr. Nguyen Ngoc Tan Luong for providing the MATLAB peak-fitting script for Raman spectroscopy and Dr. Patricia Huijbers for her valuable feedback. We also thank the Swedish Research Council (VR) (grant #2021-00613) for financial support. Finally, language polishing was assisted by ChatGPT.

Supplementary materials

Supplementary material associated with this article can be found, in the online version, at doi:10.1016/j.ensm.2025.104566.

Data availability

Data will be made available on request.

References

[1] A. Yao, S.M. Benson, W.C. Chueh, Critically assessing sodium-ion technology roadmaps and scenarios for techno-economic competitiveness against lithium-ion batteries, Nat. Energy 10 (2025) 404–416, https://doi.org/10.1038/s41560-024-01701-9.
[2] CATL Unveils Freevoy Super Hybrid Battery, Heralding a New Era of Sustainable Travel, CATL, 2024. https://www.catl.com/en/news/6301.html. accessed 20 February.
[3] J.Q. Zheng, C.H. Guan, H.X. Li, D.J. Wang, Y.Q. Lai, S.M. Li, J. Li, Z. Zhang, Unveiling the microscopic origin of irreversible capacity loss of hard carbon for sodium-ion batteries, Adv. Energy Mater. 14 (2024) 2303584, https://doi.org/10.1002/aenm.202303584.
[4] B. Sayahpour, W.K. Li, S. Bai, B.Y. Lu, B. Han, Y.T. Chen, G. Deysher, S. Parab, P. Ridley, G. Raghavendran, L.H.B. Nguyen, M.H. Zhang, Y.S. Meng, Quantitative analysis of sodium metal deposition and interphase in Na metal batteries, Energy Env. Sci. 17 (2024) 1216–1228, https://doi.org/10.1039/D3EE03141A.
[5] Z. Huang, Z. Xiao, R. Jin, Z. Li, C. Shu, R. Shi, X. Wang, Z. Tang, W. Tang, Y. Wu, A comprehensive review on liquid electrolyte design for low-temperature lithium/sodium metal batteries, Energy Env. Sci. 17 (2024) 5365–5386, https://doi.org/10.1039/D4EE02060J.
[6] P. Wen, P. Lu, X. Shi, Y. Yao, H. Shi, H. Liu, Y. Yu, Z.S. Wu, Photopolymerized gel electrolyte with unprecedented room-temperature ionic conductivity for high-energy-density solid-state sodium metal batteries, Adv. Energy Mater. 11 (2021) 2002930, https://doi.org/10.1002/aenm.202002930.
[7] Z. Wang, H. Zhang, J. Xu, A. Pan, F. Zhang, L. Wang, R. Han, J. Hu, M. Liu, X. Wu, Advanced ultralow-concentration electrolyte for wide-temperature and high-voltage Li-metal batteries, Adv. Funct. Mater. 32 (2022) 2112598, https://doi.org/10.1002/adfm.202112598.
[8] Y. Dong, P. Wen, H. Shi, Y. Yu, Z.-S. Wu, Solid-State electrolytes for sodium metal batteries: recent status and future opportunities, Adv. Funct. Mater. 34 (2024) 2213584, https://doi.org/10.1002/adfm.202213584.
[9] P. Jankowski, K. Matuszek, M. Treskow, M. Armand, D. MacFarlane, P. Johansson, Anion amphiprotic ionic liquids as protic electrolyte matrices allowing sodium metal plating, Chem. Commun. 55 (2019) 12523–12526, https://doi.org/10.1039/C9CC06083A.
[10] A. Brandt, J. Pires, M. Anouti, A. Balducci, An investigation about the cycling stability of supercapacitors containing protic ionic liquids as electrolyte components, Electrochim. Acta 108 (2013) 226–231, https://doi.org/10.1016/j.electacta.2013.06.118.
[11] Z. Cheng, Z. Zhang, F. Qiu, Z. Gao, H. Xie, Z. Xu, M. Jia, X. Zhang, H. Zhou, Regulating solvation shell to fortify anion–Cation coordination for enhanced sodium metal battery stability, ACS Energy Lett. 10 (2024) 177–184, https://doi.org/10.1021/acsenergylett.4c02751.
[12] F. Huang, P. Xu, G. Fang, S. Liang, Depth understanding of interfacial Na+ behaviors in sodium metal anode: migration, desolvation, and deposition, Adv. Mater. 36 (2024) 2405310, https://doi.org/10.1002/adma.202405310.
[13] D. De Sloovere, D.E.P. Vanpoucke, A. Paulus, B. Joos, L. Calvi, T. Vranken, G. Reekmans, P. Adriaensens, N. Eshraghi, A. Mahmoud, F. Boschini, M. Safari, M. K. Van Bael, A. Hardy, Deep eutectic solvents as nonflammable electrolytes for durable sodium-ion batteries, Adv. Energy Sustain. Res. 3 (2022) 2100159, https://doi.org/10.1002/aesr.202100159.
[14] A.S. Kelchtermans, D. De Sloovere, J. Mercken, T. Vranken, G. Mangione, B. Joos, W. Vercruysse, D. Vandamme, H. Hamed, M. Safari, E. Derveaux, P. Adriaensens, M.K. Van Bael, A. Hardy, Superconcentration strategy allows sodium metal compatibility in deep eutectic solvents for sodium-ion batteries, ACS Omega 9 (2024) 42343–42352, https://doi.org/10.1021/acsomega.4c02896.
[15] M. Kerner, N. Plylahan, J. Scheers, P. Johansson, Ionic liquid based lithium battery electrolytes: fundamental benefits of utilising both TFSI and FSI anions? Phys. Chem. Chem. Phys. 17 (2015) 19569–19581, https://doi.org/10.1039/C5CP01891A.
[16] A. Navarro-Suárez, P. Johansson, Perspective—Semi-solid electrolytes based on deep eutectic solvents: opportunities and future directions, J. Electrochem. Soc. 167 (2020) 070511. https://iopscience.iop.org/article/10.1149/1945-7111/ab68d3.
[17] P. Wróbel, P. Kubisiak, A. Eilmes, NaFSI and NaTFSI solutions in ether solvents from monoglyme to poly(ethylene oxide)—A molecular dynamics study, J. Phys. Chem. B 125 (2021) 10293–10303, https://doi.org/10.1021/acs.jpcb.1c05793.
[18] T. Shi, R. Hou, L. Zheng, H. Lu, C. Xu, X. Sun, P. He, S. Li, H. Zhou, S. Guo, Modulating double-layer solvation structure via dual-weak-interaction for stable sodium-metal batteries, Adv. Energy Mater. 15 (2025) 2405803, https://doi.org/10.1002/aenm.202405803.
[19] A. Kottarathil, Z. Slim, H.A. Ishfaq, S. Jeschke, G.Z. Żukowska, M. Marczewski, K. Lech, P. Johansson, W. Wieczorek, The role of the anion in concentrated electrolytes for lithium-sulfur batteries, J. Electrochem. Soc. 171 (2024) 070506. https://iopscience.iop.org/article/10.1149/1945-7111/ad5b8c.
[20] J. Li, S. Qin, M. Xu, W. Wang, J. Zou, Y. Zhang, H. Dou, Z. Chen, Multifunctional dual-metal-salt derived ternary eutectic electrolyte for highly reversible zinc ion battery, Adv. Funct. Mater. 34 (2024) 2402186, https://doi.org/10.1002/adfm.202402186.
[21] N.Z. Hardin, Z. Duca, A. Imel, P.A. Ward, Methyl carbamate-lithium salt deep eutectic electrolyte for lithium-ion batteries, ChemElectroChem 9 (2022) e202200628, https://doi.org/10.1002/celc.202200628.
[22] I.V. Rubtsov, K. Kumar, R.M. Hochstrasser, Dual-frequency 2D IR photon echo of a hydrogen bond, Chem. Phys. Lett. 402 (2005) 439–443, https://doi.org/10.1016/j.cplett.2004.12.083.
[23] L. Geng, X. Wang, K. Han, P. Hu, L. Zhou, Y. Zhao, W. Luo, L. Mai, Eutectic electrolytes in advanced metal-ion batteries, ACS Energy Lett. 7 (2022) 247–260, https://doi.org/10.1021/acsenergylett.1c02088.
[24] B. Aktekin, L.M. Riegger, S.-K. Otto, T. Fuchs, A. Henss, J. Janek, SEI growth on lithium metal anodes in solid-state batteries quantified with coulometric titration time analysis, Nat. Commun. 14 (2023) 6946, https://doi.org/10.1038/s41467-023-42512-y.
[25] J. Li, S. Sui, X. Zhou, K. Lei, Q. Yang, S. Chu, L. Li, Y. Zhao, M. Gu, S. Chou, Weakly coordinating diluent modulated solvation chemistry for high-performance sodium metal batteries, Angew. Chem. Int. Ed. 63 (2024) e202400406, https://doi.org/10.1002/anie.202400406.
[26] J. Chastain, R.C. King Jr, Handbook of X-ray photoelectron spectroscopy 40 (1992).
[27] D. Stottmeister, L. Wildersinn, J. Maibach, A. Hofmann, F. Jeschull, A. Groß, Unraveling propylene oxide formation in Alkali metal batteries, ChemSusChem 17 (2024) e202300995, https://doi.org/10.1002/cssc.202300995.
[28] V. Nefedov, Y.V. Salyn, G. Leonhardt, R. Scheibe, A comparison of different spectrometers and charge corrections used in X-ray photoelectron spectroscopy,

J. Electron Spectrosc. Relat. Phenom. 10 (1977) 121–124, https://doi.org/10.1016/0368-2048(77)85010-X.
[29] P. Citrin, High-resolution X-ray photoemission from sodium metal and its hydroxide, Phys. Rev. B 8 (1973) 5545, https://doi.org/10.1103/PhysRevB.8.5545.
[30] Y. He, P. Zou, S.-M. Bak, C. Wang, R. Zhang, L. Yao, Y. Du, E. Hu, R. Lin, H.L. Xin, Dual passivation of cathode and anode through electrode–Electrolyte interface engineering enables long-lifespan Li metal–SPAN batteries, ACS Energy Lett. 7 (2022) 2866–2875, https://doi.org/10.1021/acsenergylett.2c01093.
[31] C. Huang, X. Zhao, Y. Hao, Y. Yang, Y. Qian, G. Chang, Y. Zhang, Q. Tang, A. Hu, X. Chen, Long shelf-life efficient electrolytes based on trace L-cysteine additives toward stable zinc metal anodes, Small 18 (2022) 2203674, https://doi.org/10.1002/smll.202203674.
[32] L.-L. Jiang, C. Yan, Y.-X. Yao, W. Cai, J.-Q. Huang, Q. Zhang, Inhibiting solvent Co-intercalation in a graphite anode by a localized high-concentration electrolyte in fast-charging batteries, Angew. Chem. Int. Ed. 60 (2021) 3402–3406, https://doi.org/10.1002/anie.202009738.
[33] L.A. Ma, A.J. Naylor, L. Nyholm, R. Younesi, Strategies for mitigating dissolution of solid electrolyte interphases in sodium-ion batteries, Angew. Chem. Int. Ed. 60 (2021) 4855–4863, https://doi.org/10.1002/anie.202013803.
[34] Y. Ji, J. Qiu, W. Zhao, T. Liu, Z. Dong, K. Yang, G. Zheng, G. Qian, M. Yang, Q. Chen, In situ probing the origin of interfacial instability of Na metal anode, Chem 9 (2023) 2943–2955, https://doi.org/10.1016/j.chempr.2023.06.002.
[35] X. Liu, X. Zheng, Y. Dai, B. Li, J. Wen, T. Zhao, W. Luo, Suppression of interphase dissolution via solvent molecule tuning for sodium metal batteries, Adv. Mater. 35 (2023) 2304256, https://doi.org/10.1002/adma.202304256.
[36] A. Maradesa, B. Py, T.H. Wan, M.B. Effat, F. Ciucci, Selecting the regularization parameter in the distribution of relaxation times, J. Electrochem. Soc. 170 (2023) 030502. https://iopscience.iop.org/article/10.1149/1945-7111/acbca4.
[37] A. Maradesa, B. Py, J. Huang, Y. Lu, P. Iurilli, A. Mrozinski, H.M. Law, Y. Wang, Z. Wang, J. Li, Advancing electrochemical impedance analysis through innovations in the distribution of relaxation times method, Joule 8 (2024) 1958–1981, https://doi.org/10.1016/j.joule.2024.05.008.
[38] X. Xia, Y. Yang, K. Chen, S. Xu, F. Tang, L. Liu, C. Xu, X. Rui, Enhancing interfacial strength and wettability for wide-temperature sodium metal batteries, Small 19 (2023) 2300907, https://doi.org/10.1002/smll.202300907.